Supplementary Material for A numerical study of a bubble pair rising side by side in external magnetic fields

Jie ZHANG[1], Ming-Jiu NI[1,2]

[1]State Key Laboratory for Strength and Vibration of Mechanical Structures, School of Aerospace, Xi'an Jiaotong University, Xi'an, Shaanxi 710049, China

[2]School of Engineering Science, University of Chinese Academy of Sciences, Beijing 101408, China

1. Validations of the numerical methods about the MHD module implemented in Gerris

The DNS results discussed in this manuscript were obtained by using the *Gerris* code implemented with a MHD module developed by the same authors (Zhang & Ni (2014*a*,*b*)). As this code and its ability in simulating the isolated bubble rising exposed to an external MF have been documented numerously in some published papers (Zhang & Ni (2014*c*); Zhang *et al.* (2016)), we only describe more details about the specific aspects in direct relation with the present study.

The confinement effects of the computational domain on the bubble interactions are investigated first. The size of the cross - section is set as $10D \times 10D$, $20D \times 20D$ and $30D \times 30D$, respectively, while the height of the domain maintains at $60D$. By focusing on the case of a bubble pair of $D = 3$ mm, their rising paths, and the time histories of the rising velocities and collision velocities are displayed in figure 1. It is witnessed that the numerical results converge at a domain width of $L_x \geqslant 20D$, while the bouncing-separation process is affected if the lateral walls are separated by a smaller distance of $10D$. As a consequence, the computational domain is set at $20D \times 20D \times 60D$ throughout the present study.

Then we investigate the capability of the topology based AMR in resolving the thin film when the two bubbles collide, the bubble pair of $D = 2.6$ mm are investigated. Starting from a refinement of $\Delta_{bubble} = D/64$ in vicinity of the bubble interface, different strategies are adopted to further refine the meshes inside the thin film, given that $\Delta_{film} = \Delta_{bubble}/2^n$ with n denoting 0, 1, 2, et al.. Note that we suppose the two bubbles to coalesce numerically if they cannot bounce off at a refinement up to $n = 4$. The snapshots of the bubble shapes are displayed in figure 2(a), in which we observe the two bubbles coalesce at $n = 0$, 1 and 2 that a higher refinement delays the coalescence, and ultimately, they bounce off at $n = 3$ before reaching the prescribed maximum $n = 4$. As a consequence, the results indicate that the topology based AMR can delay or even prevent the numerical coalescence effectively. Then the distributions of the adaptive grid in vicinity of the interstitial film at the pre-coalescence and pre-bounce stages are presented in figure 2(b), it clearly illustrates that with an increased n, finer grids are automatically generated inside the gap between the two bubbles.

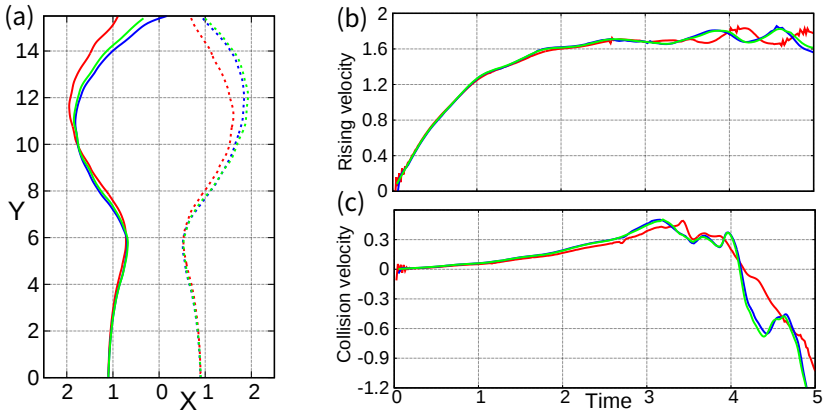

Figure 1: Confinement effects of the computational domain on the bubble interactions corresponding to $D = 3$mm. (a) Rising path; (b) rising velocity; (c) collision velocity. Red line corresponds to a domain width of $10D$, blue line is $20D$ and green line is $40D$, while the domain height maintains at $60D$.

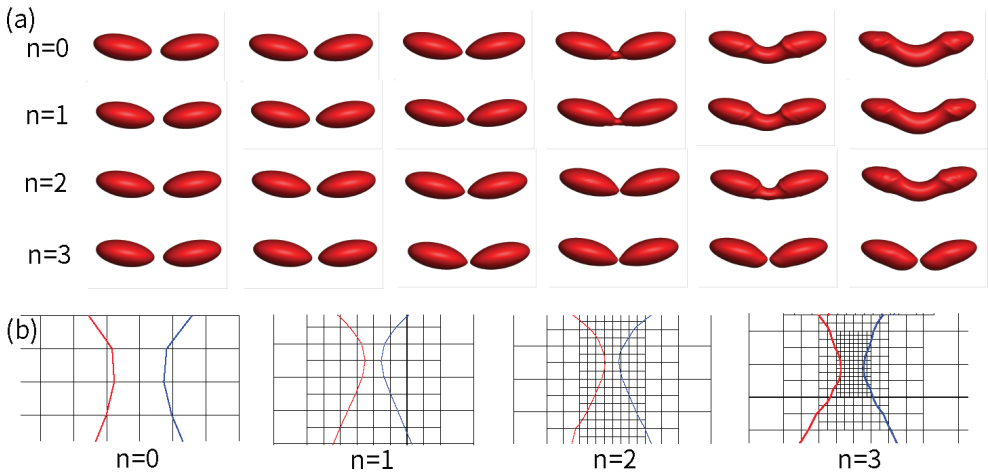

Figure 2: The capability of the topology based AMR in resolving the thin film between the two bubbles corresponding to a size of $D = 2.6$mm. (a) Snapshots of the bubble shapes under different spatial resolutions; (b) distribution of the mesh inside the thin film when the two bubbles are about to collide. In (a)(b), the value of n indicates the extra levels for the mesh being refined inside the gap, and in (b) the red line is the interface of the left bubble while the blue line is the right one. The two bubbles bounce off at a spatial resolution of $n = 3$ but coalesce numerically below that.

2. Validations of numerical method II

The diagrammer sketches of figures 6, 10 and 11 in the manuscript were obtained by using numerical method II ($NM2$), which was designed to simulate the flow past one (two) isolated frozen bubble(s), the complete incompressible MHD - Navier - Stokes equations in § 2 of the manuscript are still solved, however note that the surface tension force is now eliminated owing to the frozen shapes of the bubble(s) but no-penetration and free-slip boundary conditions are enforced on the bubble interface. Specifically, the

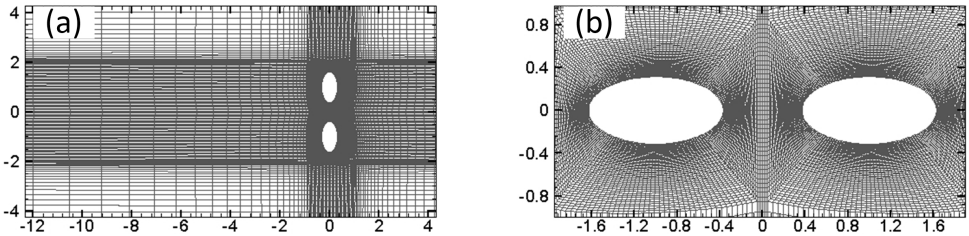

Figure 3: Spatial descretisations in the computational domain about the flow past a pair of bubbles, the thinnest meshes surrounding the bubbles have a thickness of $\delta = D/1000$ while the growth factor is $\varepsilon = 1.1$. (a) Overall view; (b) local view.

normal velocity vanishes due to the impermeability of the interface, and the tangential components of fluid shear stress on the bubble surface are specified to zero:

$$\boldsymbol{u} \cdot \boldsymbol{n} = 0 \tag{2.1}$$

$$(\mathbb{S} \cdot \boldsymbol{n}) \cdot \boldsymbol{s} = 0 \tag{2.2}$$

$$(\mathbb{S} \cdot \boldsymbol{n}) \cdot \boldsymbol{t} = 0 \tag{2.3}$$

where $\mathbb{S} = \mu(\nabla \boldsymbol{u} + \nabla^T \boldsymbol{u})$ is the viscous stress tensor, $\boldsymbol{n}$ is the outward unit normal vector of the bubble interface, and $\boldsymbol{s}$ and $\boldsymbol{t}$ are two mutually orthogonal unit vectors tangential to the bubble interface.

With respect to the numerical methods, the convective and diffusive terms are spatially discretized by using second-order accurate center difference schemes, which are implemented with skewness corrections for the non-orthogonal meshes. Then a fraction-step method is employed to solve the pressure-velocity coupling equation. The temporal discretisations are as follows, an Adams - Bashforth scheme is designed to update the convective term and a Crank-Nicolson scheme is for the diffusive term.

In the simulations, the bubble(s) is located in a computational domain characterised by a size of $L_x \times L_z \times L_y = 20D \times 20D \times 40D$ with $x-$ connecting the bubble centroid and $y-$ denoting the streamwise direction. Non-uniform body-fitted meshes are generated around the bubble(s), their typical distributions corresponding to a bubble pair of $Re = 300$ and $\chi = 2.0$ are displayed in figure 3. Note that the thinnest meshes surrounding the bubbles have a thickness of $\delta = D/1000$ while the growth factor is $\varepsilon = 1.1$, then the domain is discretisized by $128 \times 81 \times 96$ nodes. Pan *et al.* (2018, 2019) already show that such spatial resolutions are sufficient in resolving the boundary layer about a MHD flow past a rigid sphere at Reynolds number up to 300, and as a consequence, neither the grid independent study nor the numerical validations about the MHD module will be discussed here.

Instead, we mainly focus on the free-slip boundary problems, which correspond to equations (2.1) $\sim$ (2.3). Two series of tests are carried out, one is about the drag coefficients for different hydrodynamic flows past an isolated ellipsoidal bubble, and the results provided by Blanco & Magnaudet (1995) are used for comparison, as presented in Table 1. The other is about the hydrodynamic forces acting on spherical bubble pairs rising side by side with a separated distance of $S = 1.5D$, and the comparisons against the numerical results reported by Legendre *et al.* (2003) are given in Table 2. Note that the Reynolds number here is characterised by the length of the major axe given by b at $\chi > 1$, and the drag or lift coefficient is defined as $C_{D,L} = 8F_{y,x}/\pi b^2 \rho U_0^2$, with $F_{y,x}$ being the total forces in the corresponding direction. Both series of tests show very good agreements

χ	Re	100	400	600	800
1.5	Present	0.512	0.163	0.114	0.085
	Blanco & Magnaudet (1995)	0.516	0.161	0.112	0.084
1.95	Present	0.631	0.222	0.155	0.115
	Blanco & Magnaudet (1995)	0.627	0.220	0.152	0.117

Table 1: Drag coefficient C_D of an ellipsoidal inviscid bubble as a function of Re and χ. Note Re is characterised by the length of the major axe given by b.

Re	Results	C_D	C_L
10	Present	2.50	0.158
	Legendre *et al.* (2003)	2.53	0.160
300	Present	0.147	−0.0662
	Legendre *et al.* (2003)	0.147	−0.0664

Table 2: Drag and lift coefficients of a pair of spherical bubbles separated by a distance of $S = 1.5D$.

with reference results, and as a consequence, the accuracy of $NM2$ in simulating the flow past bubble(s) is identified, and the combination with the aforementioned MHD module enables it to be credible in simulating the MHD flows past bubble(s).

3. Snapshots of vortex structures using streamwise component and λ_2 criterion

As a supplement of figure 4 in the manuscript, a complete evolution of the vortex structures corresponding to different bubble pairs are displayed in figure 4 and 5, with the previous describing the streamwise component of $\omega_y = \pm 4$ while the later using the λ_2 criterion(Jeong & Hussain (1995)) of $\lambda_2 = -0.2$. Note that the picked time period is very short, i.e. for $D = 2$ mm, the starting dimensionless time moment is $t_0 = 2.76$ with an interval of $\Delta t = 0.035$ ($\Delta Y < 0.07$) between two successive pictures, and others are $t_0 = 2.90$ and $\Delta t = 0.066$ for $D = 2.5$ mm, $t_0 = 2.90$ and $\Delta t = 0.13$ for $D = 3.0$ mm, and $t_0 = 2.12$ and $\Delta t = 0.71$ for $D = 4.0$ mm. In each panel, the wake vortices are only displayed in every two pictures while the other one only portrays the bubble shapes.

4. Rising paths of the bubble pairs under different MFs

As a supplement of figure 7, 12 and 14 in the paper, a complete set of rising paths for the bubble pair exposed to different MFs are plot in figure 6, 7 and 8, which correspond to the streamwise MFs, the transverse MFs and the spanwise MFs, respectively. Besides, the snapshots of the bubble shapes are also displayed during the collision period, which is rather short that the bottom image denotes $t_0 = 2.61$ while the time interval between two successive pictures $\Delta t = 0.334$. In both of streamwise MFs and transverse MFs, we see the bouncing-separation interaction transits to coalescence gradually by promoting the MF strength, however, in a spanwise MF, a transition from bounce to coalescence is firstly observed within a small-to-moderate MF until $N_x = 0.2$, but then a continuous promotion of N_x makes the two bubbles bounce ($N_x = 0.8$) and even repel ($N_x = 2.24$).

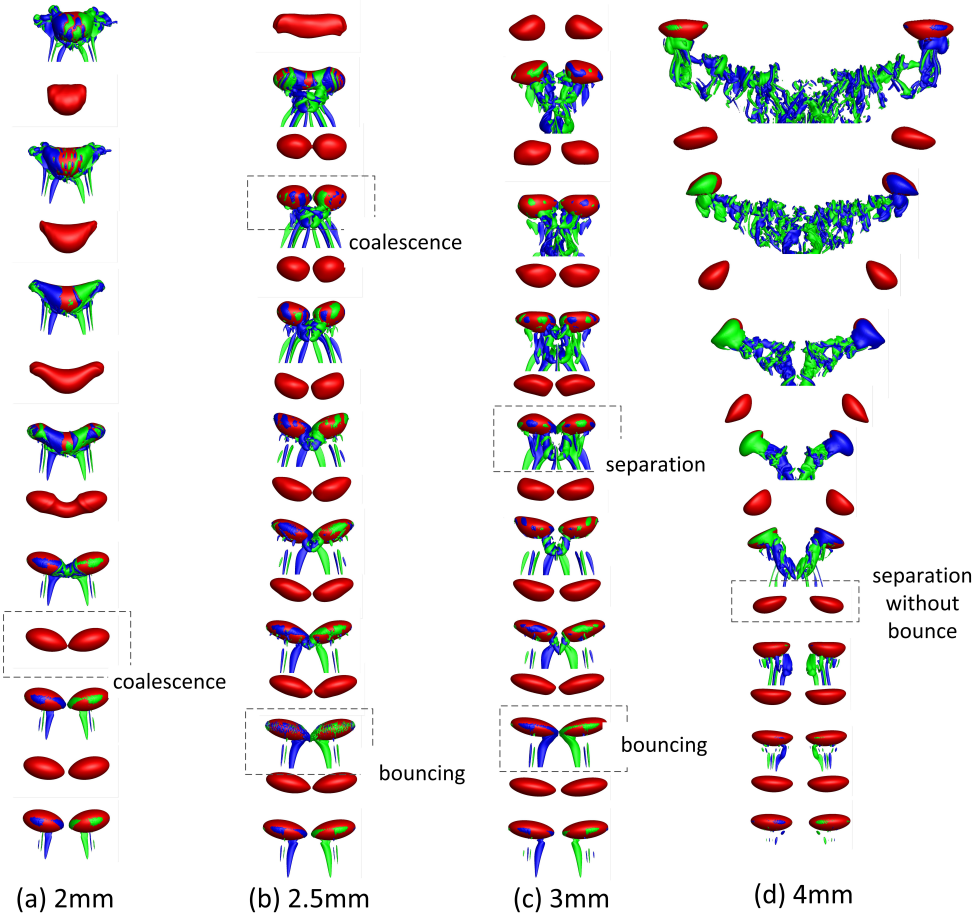

Figure 4: Snapshots of the wake vortices $\omega_y = \pm 4$ during the bubble interactions corresponding to (a) $D = 2$ mm, (b)$D = 2.5$ mm, (c) $D = 3$ mm and (d) $D = 4$ mm.

5. Evolution of the vortex structures corresponding to $N_x = 0.80$ and 2.24

Figure 9(a) displays the snapshots of the double-threaded vortices behind the bubble pairs at a moderate spanwise MF of $N_x = 0.80$, with the first two embed pictures denoting iso-contours $\omega_y = \pm 1.7$ for a better illustration of Lorentz diffusion induced vortices and the following embed pictures are $\omega_y = \pm 3.5$. Clearly, before $t = 11$ when the two bubbles are separated with a relatively far distance, Lorentz diffusion induced vortices are dominant that little asymmetry is observed between L1(2) and R1(2). However as the two bubbles keep on approaching within $11 < t < 23$, the double vortex pairs become more asymmetrical that more fluids converge to the interior position to generate stronger vortex pair there, which finally generate repulsive lift force to make the two bubbles bounce off. In addition, figure 9(b) describes the evolution of the double-threaded vortices $\omega_y = \pm 3.5$ corresponding to a strong spanwise Mf of $N_x = 2.24$. We see the two bubbles never approach towards each other, because the asymmetric double vortex pairs, which

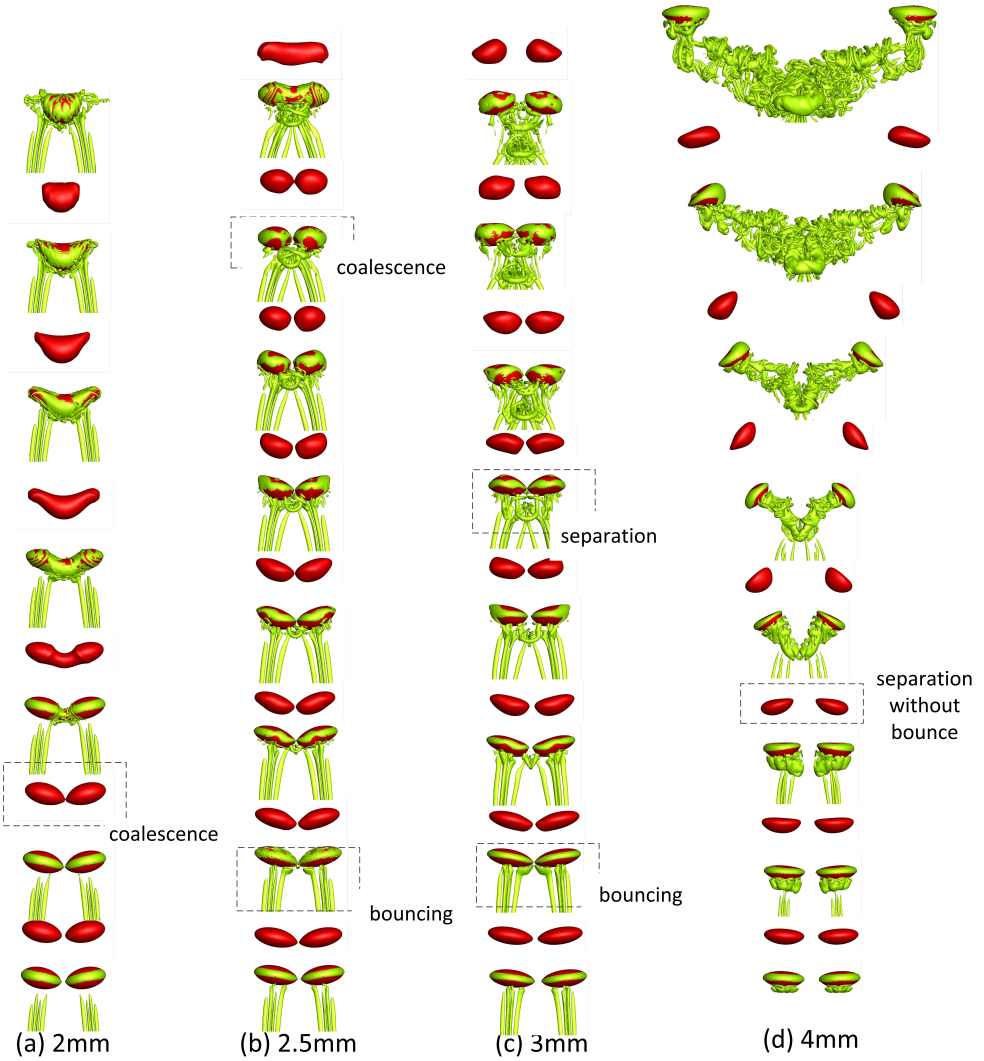

Figure 5: Snapshots of the wake vortices $\lambda_2 = -0.2$ (Jeong & Hussain (1995)) during the bubble interactions corresponding to (a) $D = 2$ mm, (b)$D = 2.5$ mm, (c) $D = 3$ mm and (d) $D = 4$ mm.

are induced by the Lorentz diffusion effect, produce a repulsive force which prevails over the weak attractive force in this case from the beginning of rising.

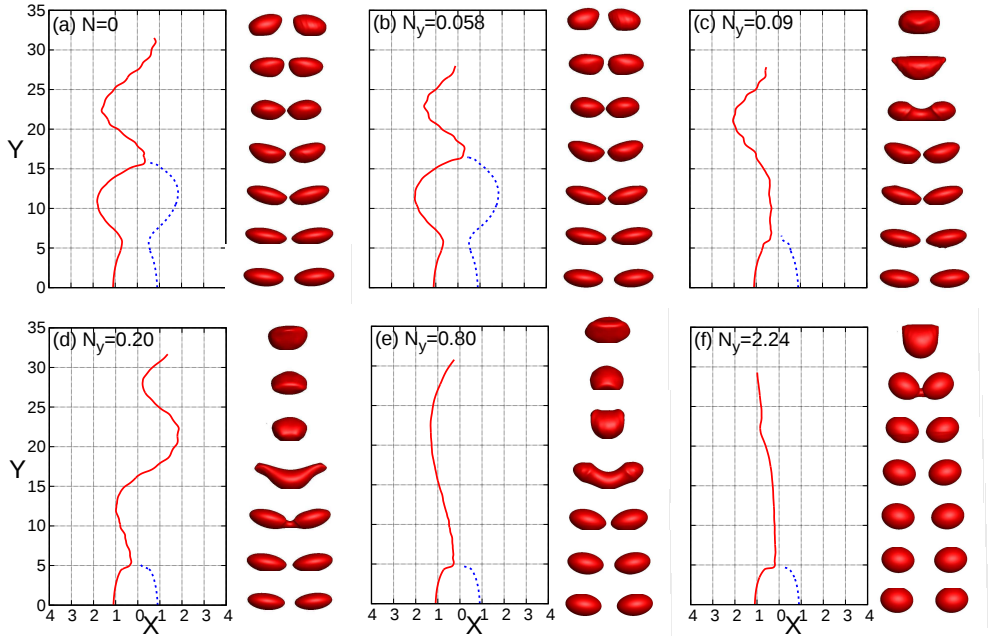

Figure 6: Rising paths of the bubble pairs exposed to different streamwise MFs ranging between $N = 0$ and $N_y = 2.24$, and the bubble size is fixed at $D = 3.0$ mm. Snapshots of the bubble shapes are also displayed in the right panel, with the bottom image denoting $t_0 = 2.61$ and the time interval between two successive pictures $\Delta t = 0.334$. With an intensified streamwise MF, the interaction between the bubble pair transits from bouncing-separation to bouncing-coalescence, and then direct coalescence.

REFERENCES

Blanco, Armando & Magnaudet, Jacques 1995 The structure of the axisymmetric high-reynolds number flow around an ellipsoidal bubble of fixed shape. *Physics of Fluids (1994-present)* **7** (6), 1265–1274.

Jeong, Jinhee & Hussain, Fazle 1995 On the identification of a vortex. *Journal of fluid mechanics* **285**, 69–94.

Legendre, Dominique, Magnaudet, Jacques & Mougin, Guillaume 2003 Hydrodynamic interactions between two spherical bubbles rising side by side in a viscous liquid. *Journal of Fluid Mechanics* **497**, 133–166.

Pan, Jun-Hua, Zhang, Nian-Mei & Ni, Ming-Jiu 2018 The wake structure and transition process of a flow past a sphere affected by a streamwise magnetic field. *Journal of Fluid Mechanics* **842**, 248–272.

Pan, Jun-Hua, Zhang, Nian-Mei & Ni, Ming-Jiu 2019 Wake structure of laminar flow past a sphere under the influence of a transverse magnetic field. *Journal of Fluid Mechanics* **873**, 151–173.

Zhang, Jie & Ni, Ming-Jiu 2014*a* A consistent and conservative scheme for mhd flows with complex boundaries on an unstructured cartesian adaptive system. *Journal of Computational Physics* **256**, 520–542.

Zhang, Jie & Ni, Ming-Jiu 2014*b* Direct simulation of multi-phase mhd flows on an unstructured cartesian adaptive system. *Journal of Computational Physics* **270**, 345–365.

Zhang, Jie & Ni, Ming-Jiu 2014*c* Direct simulation of single bubble motion under vertical magnetic field: Paths and wakes. *Physics of Fluids (1994-present)* **26** (10), 102102.

Zhang, Jie, Ni, Ming-Jiu & Moreau, René 2016 Rising motion of a single bubble through a liquid metal in the presence of a horizontal magnetic field. *Physics of Fluids* **28** (3), 032101.

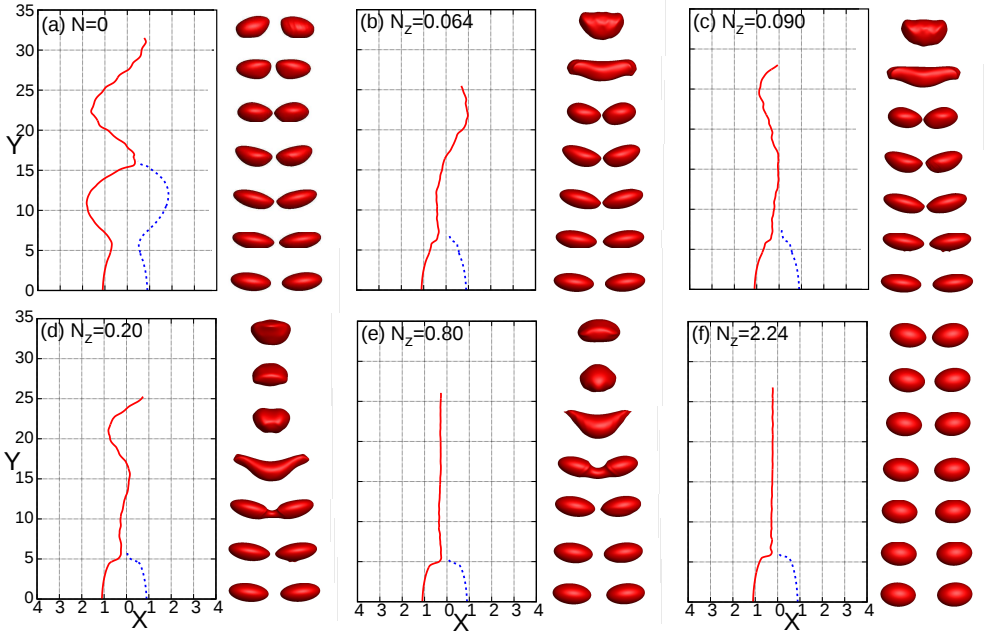

Figure 7: Rising paths of the bubble pairs exposed to different transverse MFs ranging between $N = 0$ and $N_z = 2.24$, and other descriptions refer to those in the caption of figure 6.

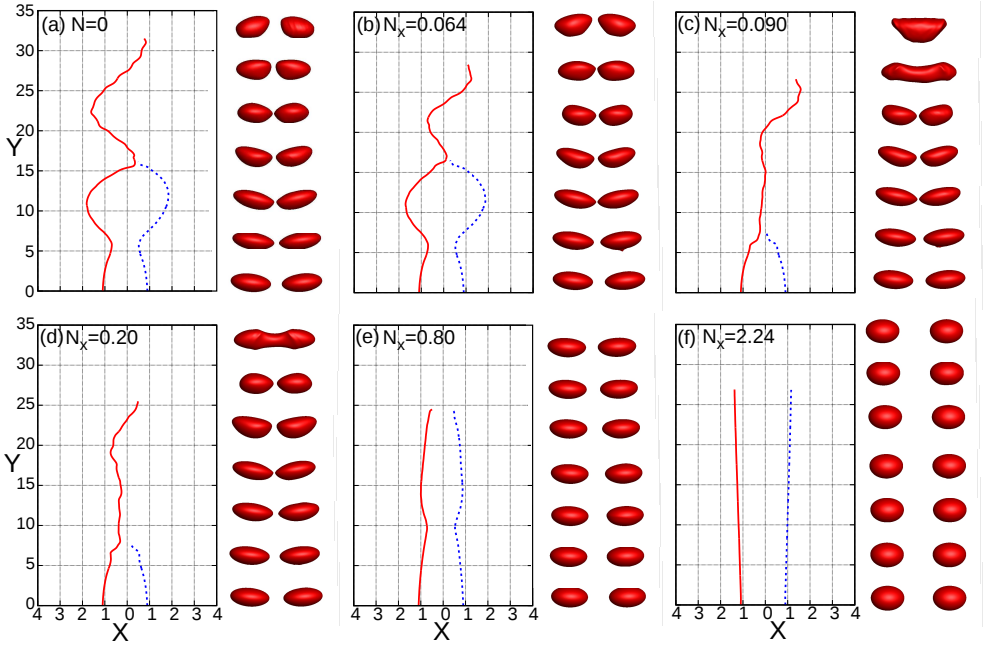

Figure 8: Rising paths of the bubble pairs exposed to different spanwise MFs ranging between $N = 0$ and $N_x = 2.24$, and other descriptions refer to those in the caption of figure 6.

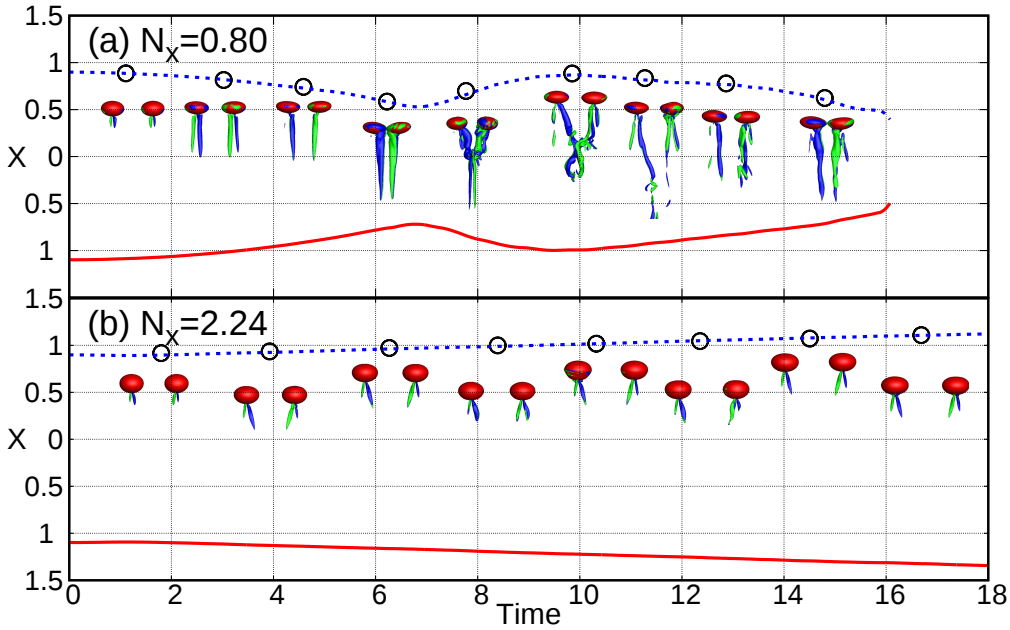

Figure 9: Time histories of the double-threaded vortices behind the bubble pair corresponding to (a) $N_x = 0.80$ and (b) $N_x = 2.24$. Except that the first two embed figures in (a) denote the iso-contours $\omega_y = \pm 1.7$, all others correspond to $\omega_y = \pm 3.5$.